Vacuum Drying of Wood with Radiative Heating: II. Comparison between Theory and Experiment

Ian W. Turner
School of Mathematical Sciences, Queensland University of Technology, Brisbane, Q4001, Australia

Patrick Perré
ENGREF/LERMAB, Laboratory of Wood Sciences, UMR INRA/ENGREF/UHP F-54042 Nancy, Cedex, France

In part I of this work extensive experimental data sets for the vacuum drying of wood with radiative heating were presented for sapwood and heartwood of different species (Picea abies, Abies alba, and Fagus silvatica). These data sets are used here to validate two previously developed drying models. The first drying model, which is known as TransPore, is a comprehensive model able to capture the intricately coupled heat- and mass-transfer mechanisms that evolve throughout the drying process. The second model, which is known as Front_2D, uses a number of simplifying assumptions to reduce the complexity of the comprehensive model to a system that enables a semianalytical approach to be exploited for its solution. Although the first model provides a more accurate description of the entire process, the second model is able to produce representative solutions very efficiently in terms of overall computational times, making it a viable option for on-line control purposes. The comparison with experimental data highlights that both models are able to capture all of the observed trends, allowing them to be used with confidence for investigating the vacuum drying process at a fundamental level. The new contribution of this work lies in the fact that both models are used here for the first time to simulate drying at a reduced external pressure. © 2004 American Institute of Chemical Engineers *AIChE J,* 50: 108–118, 2004

Keywords: vacuum drying simulations, heat and mass transport mechanisms, transPore, front_2D

Introduction

Over the last two decades the simulation of wood drying has been the subject of much research impetus, and it is clear that the field is truly interdisciplinary, with key articles found in top engineering, wood science, and mathematical journals. These publications cover a wide range of diverse topics, including the derivation of the physical and mechanical formulation, the development of analytical and numerical solutions, the determination of the physical and mechanical characterization of the medium being dried, and the process experiments carried out on both laboratory and industrial scales. Nowadays, as a result of ever-increasing computational power, numerical simulation has fast become a very powerful tool that drying practitioners can use to study the drying process at a fundamental level. Such knowledge has guided the introduction of many new and innovative drying operations into the industrial sector. Nevertheless, it is the opinion of the authors that a close interaction still must exist between drying theoreticians and practitioners, because of the complexity of a global strategy for wood-drying improvement, or kiln control, that must address a range of important issues. In particular, the final choice of the modeling approach must take into consideration an extensive list, which includes the choice of the most appropriate numerical model

Correspondence concerning this article should be addressed to P. Perré at perre@engref.fr.

for the study, the knowledge of the important product properties needed for the simulations, and whether all of the required physical parameters are available and if not, whether it is possible to perform or propose measurements for the unknown properties.

The literature highlights several sets of macroscopic equations being used to model the drying process. The first fundamental difference between the underlying mathematical models lies in the number of state variables used to describe the process. Three possibilities exist, which are known as one-variable, two-variable, or three-variable models. A one-variable model typically uses moisture content as the primary variable or an equivalent variable, such as saturation or water potential. Two-equation models use both moisture content (or its equivalent) and temperature, T, or an equivalent variable such as enthalpy, in the formulation, and the most sophisticated three-equation models use moisture content (or its equivalent), T (or its equivalent), and gaseous pressure P_g, or an equivalent variable such as air density or intrinsic air density. Perré (1999) gives a critical review of the possibilities and limitations given by these different sets of equations. The use of moisture content alone is the basis of many correlations of lumber-drying rates (see Keey et al., 2000). Doe et al. (1996) found that at the relatively low temperatures ($<40°C$) used in drying eucalyptus hardwoods, both moisture content and temperature are needed to describe the movement of moisture. The importance of the role of gaseous pressure appears in the simulation of high-temperature seasoning, vacuum drying, or microwave drying (Perré and Degiovanni, 1990; Turner and Perré, 1996; Perré and Turner, 1999a,b). As a general rule, a one-variable model should be avoided, because it is not able to account for the very important coupling between heat and mass transfer that exists during drying. A two-variable model is appropriate for most of the drying conditions encountered in industry. Finally, the quite complex three-variable model should be reserved for processes during which the internal pressure has a significant impact on internal moisture transport, such as the processes with internal vaporization that include vacuum drying, high-temperature drying, and radiofrequency drying.

The second fundamental difference between the drying models lies in the number of spatial dimensions used to describe the process. One-dimensional (1-D) models that use the thickness of the sample as the only spatial dimension are fast running and allow the most important transport phenomena to be captured, including, for example, transfers and drying stress. For a refined approach, a 2-D model can be useful where the thickness and the width of the sample are used in the formulation to enable a better evaluation of the drying rate and stress development. Moreover, such models can account for the grain direction and the presence of both sapwood and heartwood in wood. Due to the large anisotropy ratios evident in wood, the length of the sample is absolutely required in the case of processes where internal vaporization is important. Finally, a 3-D model allows a comprehensive geometrical modeling to be investigated (Perré and Turner, 1999b).

Once the specific formulation has been decided, various approaches in the computational solution strategy can be adopted to simulate the drying process. For example, simple and efficient methods that use the assumption of constant physical parameters can be used to address specific problems, including kiln sizing and the global effect of the product size. Among these methods, the dimensionless drying curves proposed by Van Meel (1958) or the simple analytical solutions outlined by Crank (1975) have to be noted. However, the development of these methods fails to provide a complete understanding of the internal transfer mechanisms and the coupling that always exists between heat and mass transfer.

A second set of computational strategies can be used that try to be more realistic by using a more suitable set of simplifying assumptions. All models based on the concept of "drying front" belong to this category (Hadley, 1982; Rogers and Kaviany, 1992; Perré et al., 1999). Finally, all computational models based on a complete numerical solution of the nonlinear conservation laws constitute the third category. The first representative examples of this category appeared more than 20 years ago (Bramhall, 1979; Kawai, 1980). Thereafter, a more comprehensive physical formulation has been applied with success, at first in one-dimension (Stanish et al., 1986; Moyne, 1987; Ben Nasrallah and Perré, 1988; Ilic and Turner, 1989) and later in two-dimensions (Perré and Degiovanni, 1990; Fyhr and Rasmuson, 1996; Boukadida and Ben Nasrallah, 1995; Pang, 1996). Nowadays, as a result of the significant advancements in numerical techniques, including efficient inexact Newton iterative solvers and the use of unstructured meshes, together with the ever-increasing power of computers, the numerical simulations have become a real tool, able to deal with a comprehensive formulation with any geometrical formulation (Turner and Perré, 1996; Perré, 1999a,b). Before going further, one has to note that the vacuum drying of wood involves two particular and important features:

(1) The accelerated internal mass transfer due to the overpressure that can exist within the product;

(2) The effect of the high anisotropy ratio of wood permeability (from 100 to more than 10^4), especially for wood with a high aspect ratio between the length and width of the sample. No realistic simulation can be expected from a model that is not able to account for these two important features.

The objectives of Part II of this research are to use the extensive experimental data sets documented in Part I for the purposes of assessing the accuracy and predictive ability of two previously developed drying models. The first model is a comprehensive drying model known as *TransPore* (Turner and Perré, 1996; Perré and Turner, 1999a,b), which is able to capture the quite subtle and convoluted heat- and mass-transfer mechanisms that evolve throughout the drying process. The second drying model, which is known as *Front_2D* (Perré et al., 1999), uses a number of simplifying assumptions to reduce the complexity of the comprehensive model to a system that enables a semianalytical approach to be exploited for its solution. Although the physical formulation used in both of these models always had the capability of simulating any external pressure applied to the medium, this is the first time that they are actually used at an external pressure different from the atmospheric value. Specific differences in the two formulations for vacuum drying will be elucidated in the following sections of the text.

Comprehensive Drying Code *TransPore*

The macroscopic conservation equations that govern the heat- and mass-transfer phenomena that arise in porous media during drying are now well known (Whitaker, 1998). This

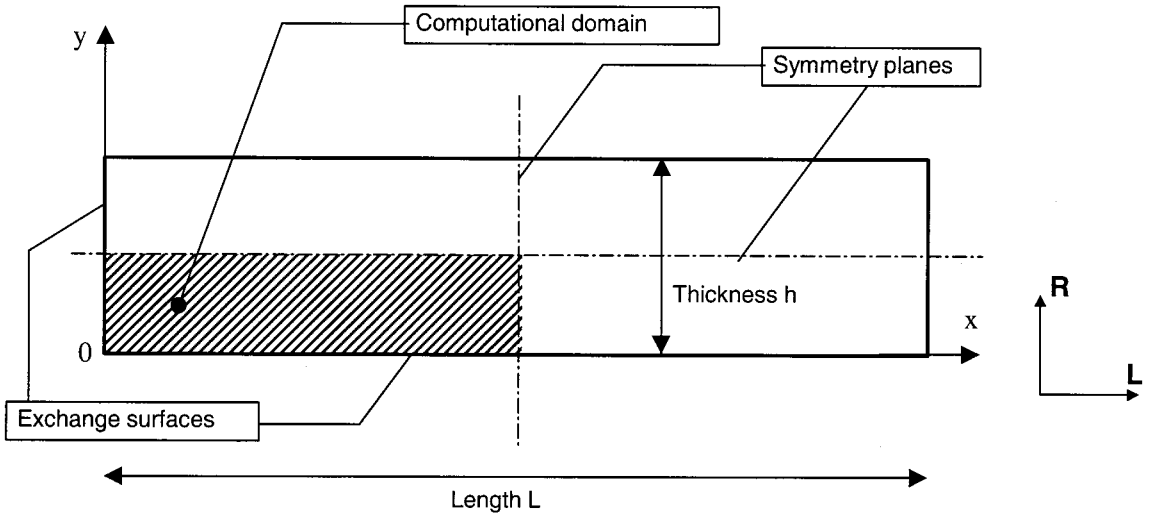

Figure 1. The 2-D drying configuration considered in this work.

formulation has been successfully adapted and applied to several configurations of wood drying, including processes that involve intense mass transfer due to the generation of an important internal overpressure within the medium (Perré and Degiovanni, 1990; Perré et al., 1993; Perré and Turner, 1996, 1999a,b). The important details of the drying transport equations are summarized in the following paragraphs and the reader is referred to previous work by the authors for a complete description of the underlying model.

Water Conservation.

$$\frac{\partial}{\partial t}\left(\epsilon_\ell \rho_\ell + \epsilon_g \rho_v + \bar{\rho}_b\right) + \nabla \cdot \left(\rho_\ell \bar{\boldsymbol{v}}_\ell + \rho_v \bar{\boldsymbol{v}}_g + \underline{\rho_b \boldsymbol{v}_b}\right) = \nabla \cdot \left(\rho_g \overline{\bar{D}}_{\text{eff}} \nabla \omega_v\right) \quad (1)$$

Energy Conservation.

$$\frac{\partial}{\partial t}\left(\epsilon_\ell \rho_\ell h_\ell + \epsilon_g(\rho_v h_v + \rho_a h_a) + \bar{\rho}_b \bar{h}_b + \bar{\rho}_o h_s - \epsilon_g P_g\right) + \nabla \cdot \left(\rho_\ell h_\ell \bar{\boldsymbol{v}}_\ell + (\rho_v h_v + \rho_a h_a)\bar{\boldsymbol{v}}_g + h_b \underline{\rho_b \boldsymbol{v}_b}\right) = \nabla \cdot \left(\rho_g \overline{\bar{D}}_{\text{eff}}(h_v \nabla \omega_v + h_a \nabla \omega_a) + \overline{\bar{K}}_{\text{eff}} \nabla T\right) + \Phi \quad (2)$$

Air Conservation.

$$\frac{\partial}{\partial t}\left(\epsilon_g \rho_a\right) + \nabla \cdot \left(\rho_a \bar{\boldsymbol{v}}_g\right) = \nabla \cdot \left(\rho_g \overline{\bar{D}}_{\text{eff}} \nabla \omega_a\right). \quad (3)$$

In these equations, the velocities of the gaseous and liquid phases are, respectively, expressed using the generalized Darcy's law

$$\bar{\boldsymbol{v}}_i = -\frac{\overline{\bar{K}}_i \overline{\bar{k}}_i}{\mu_i} \nabla \varphi_i, \nabla \varphi_i = \nabla P_i - \rho_i g \nabla \chi \qquad \text{for} \quad i = \ell, g \quad (4)$$

where the quantities φ are known as the phase potentials, and χ is the depth scalar. All other symbols have their usual meaning. The liquid and gaseous pressures are related through the capillary pressure. The latter is assumed to be dependent upon only the moisture content

$$P_\ell = P_g - P_c(X) \quad (5)$$

The two-dimensional drying configuration under study here is exhibited in Figure 1, where for the log under consideration here, due to axial symmetry, a single radial-longitudinal plane is computed. The specific boundary and initial conditions necessary to close the model are presented in the next subsection.

Boundary and Initial Conditions. There are two types of boundary conditions that need to be discussed, namely, conditions at the external boundaries, and conditions at symmetry planes (refer again to Figure 1). The boundary conditions proposed for the external drying surfaces of the sample are assumed to be of the following form

$$\boldsymbol{J}_v \cdot \hat{\boldsymbol{n}} = k_m c M_v \ln\left(\frac{1 - x_{ch}}{1 - x_v}\right)$$

$$\boldsymbol{J}_e \cdot \hat{\boldsymbol{n}} = h(T - T_{ch}) + \epsilon\sigma(T^4 - T_{\text{eq}}^4) + h_v k_m c M_v \ln\left(\frac{1 - x_{ch}}{1 - x_v}\right) \quad (6)$$

where $\boldsymbol{J}_v$ and $\boldsymbol{J}_e$ represent the fluxes of total moisture and total enthalpy at the boundary, respectively, and σ is the Stefan-Boltzmann constant. The equivalent emissivity factor, ϵ, and the equivalent temperature, T_{eq}, are calculated using a simple energy balance

$$\epsilon\sigma(T^4 - T_{\text{eq}}^4) = \epsilon_s \epsilon_{ch} f_{s \to ch} \sigma(T^4 - T_{ch}^4) + \epsilon_s \epsilon_{IR} f_{s \to IR} \sigma(T^4 - T_{IR}^4) \quad (7)$$

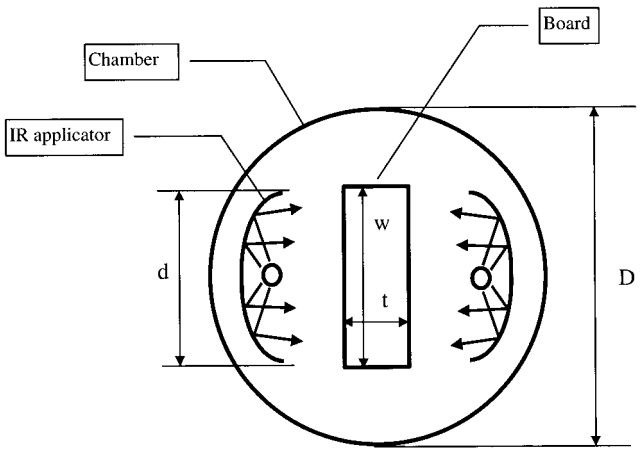

Figure 2. Evaluation of the shape factors: at midlength of the board.

In Eq. 7, the actual view factors $f_{s\rightarrow ch}$ and $f_{s\rightarrow IR}$ (see Figure 2) have been estimated from Bird et al. (1960) for the case of two parallel metal plates. Here, ϵ stands for the emissivity factors, and the subscripts s, ch and IR indicate the exchange surface, chamber, and IR emitters, respectively.

The total pressure at the external drying surfaces is fixed at the vacuum chamber pressure, P_{ch}. Recalling that one of the primary variables used for the computations is the averaged air density, the Dirichlet boundary condition $P_g = P_{ch}$ has to be modified to form an appropriate nonlinear equation for this primary variable, namely

$$\epsilon_g(P_v - P_\infty) + \frac{\bar{\rho}_a RT}{M_a} = 0 \tag{8}$$

where $\epsilon_g = \phi(1 - S_w)$ is the volume fraction of the gaseous phase, which can be determined from the computed moisture content at the surface of the board. One must note here the real value of the full Newton procedure of the drying system; here Eq. 8 is simply resolved together with all of the other nonlinear discrete nodal conservation laws at every time step. The authors feel that the use of the Newton methodology is absolutely essential in the successful implementation of the vacuum drying model discussed here.

Initially, the porous medium has some prescribed moisture content (any radial profile), with the pressure and temperature being constant throughout the board at the atmospheric value and initial temperature, respectively.

Numerical Solution Procedure. The numerical procedure used to resolve the drying model has been published extensively over the last decade, and the interested reader is referred to some of the more recent publications of the authors for the finer details (Turner and Perré, 1996; Perré and Turner, 1999a,b). Briefly, the *finite volume* method is implemented on a structured mesh to discretize the conservation laws. Thereafter, an efficient inexact Newton method is used to resolve in time the complicated and often large nonlinear system that describes the drying process. Flux limiting is used for the spatial weighting schemes for all advection/convection terms in the equations in order to reduce numerical dispersion of the drying fronts, and the introduction of the fixed phase ensures that full saturation $S_w = 1$ is never reached at the surface of the medium. These are important advancements in the numerical treatment of the computational model *TransPore* that can enhance convergence of the nonlinear iterations and ensure accurate resolution of the drying fronts on relatively coarse meshes [see Turner and Perré (2001) for a further discussion of these issues] and are particularly useful for simulating the vacuum drying process.

In order to be consistent with the actual volumetric flux of the vacuum pump used in the experiment, the chamber pressure is assumed to decrease steadily from the initial atmospheric value to the vacuum chamber operating pressure of $P_{ch} = 0.2P_{atm}$ over a period of 10 min. During this period, the air is removed from the chamber and the vapor pressure at the surface of the board must be regulated carefully to ensure convergence of the model. It should be noted that in the case of pure vapor within the chamber, the boundary condition (Eq. 6) imposes an equality of the wood surface vapor pressure and the vacuum chamber vapor pressure due to the singularity that arises in the logarithm. Great care must be taken with the treatment of this singularity in order to avoid problems with numerical floating-point overflow in this situation. We choose a representative value for the heat- and mass-transfer coefficients for use throughout the simulations.

The 2-D Semi-Analytical Model Front_2D

Keeping in mind the complexity of the coupled heat and mass transfer that occur during drying, it must be clear to the reader that the analytical model discussed in the following paragraphs is based on an "intelligent" set of simplifying assumptions. The real challenge is, as is usual in science, to find a good compromise between how difficult it is to solve the governing set of equations, on the one hand, and the variety of configurations that the new model can handle, on the other hand. A detailed presentation of this solution strategy can be found elsewhere (Perré et al., 1999). Referring to Figure 3, the main assumptions and the final set of equations are described hereafter.

Two-Dimensional Pressure Field. Assumptions A1 to A5 allow the two-dimensional pressure field to be resolved in terms of an analytical expression:

A1. The present model uses the basic assumption of a drying front, which implies that the zone where liquid evaporates to water vapor is reduced to a line in two-dimensions. Because the model is 2-D, the product shape is assumed to be rectangular, with thickness ℓ and length L. The front position is assumed to be parallel to the exchange surface. Denote e the distance between the front and the exchange surface and c the complementary distance, $c = \ell - e$ (see Figure 3).

A2. It is assumed that the gaseous phase consists only of water vapor in the zone between the front and the exchange surface.

A3. The water vapor is assumed to migrate only according to Darcy's law. Consequently, the diffusion term is neglected, which is consistent with assumption A2.

A4. The porous medium is divided into two zones: one vapor zone and one liquid zone. Within each zone, the physical parameters are assumed constant in space.

A5. The pressure field is assumed to have reached the steady state. Indeed, due to the ratio of liquid density over the

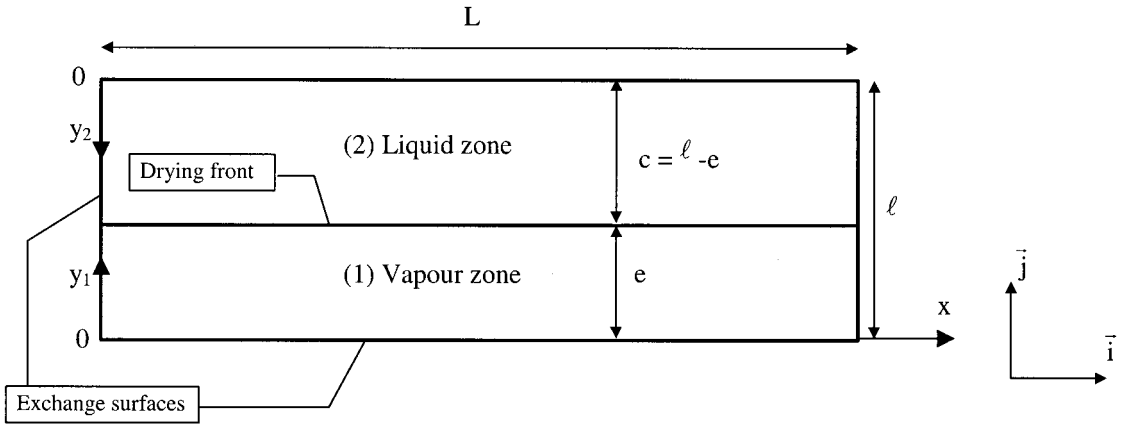

Figure 3. The drying configuration that results from the physical assumptions of the 2-D analytical model.

vapor density, the front migration is always small compared to the gas velocity.

Energy Balance. Two additional assumptions allow the temperature field within the medium to be governed by a very simple 1-D and linear, differential equation:

A6. The heat transfer within the medium is assumed to occur only in the thickness of the product. Indeed, the anisotropy ratio, which can be substantial for permeability, is often much lower for thermal conductivity.

A7. The heat required to change the product temperature (sensible heat) is negligible.

Liquid Migration. The simulation of the process requires the front position e to be connected to the averaged moisture content. Keeping in mind the aim of this work, which is to obtain a realistic but simplified model, two further assumptions are proposed to describe the way in which the liquid migrates within the medium:

A8. The liquid propagates only in the thickness of the product. This means that, concerning the liquid flow, the capillary forces remain larger than the additional driving force generated by the overpressure. A one-dimensional moisture content profile results from this hypothesis.

A9. The 1-D moisture content profile has a quadratic shape. Its derivative on the plane of symmetry (at $y_1 = \ell$) or at the initial moisture content is equal to zero. At the exchange surface (during the first drying period), or at the front position (during the second drying period), the moisture content gradient is related to the liquid flux through the liquid migration coefficient:

The Final Set of Equations. The complete solution allows the calculation of the two-dimensional pressure field resulting from a constant source $\langle q_m \rangle$ located at the front position to be determined all over the sample. Remaining consistent with the physical assumption, this pressure field depends linearly on the flux $\langle q_m \rangle$. The most important result of this calculation is the possibility to observe and to model very quickly the effect of the configuration: length, thickness, front position, anisotropy ratio, and the difference of permeability between the liquid and the vapor zones are all included within the expression for the solution

$$\langle q_m \rangle = -\rho_v \frac{K_{1y}}{\mu_v} \left(\frac{e}{\beta}\right) \frac{\Delta P}{e},$$

with

$$\beta = \sum_{k=1}^{\infty} \frac{2(-1)^k}{\alpha_k^2 L^* \{\coth(\alpha_k e) + (A_2/A_1)\tanh(\alpha_k c)\}} \tag{9}$$

and

$$L^* = \frac{L}{\sqrt{\gamma}} \qquad \gamma = \frac{K_{1x}}{K_{1y}} \neq 0$$

$$\alpha_k = \left(\frac{2k+1}{2L^*}\,\pi\right) \qquad \text{and} \qquad c = \ell - e \tag{9}$$

where ΔP is the center overpressure (pressure at the front position and at the dimensionless mid-length, L^*, minus the external pressure).

In Eq. 9, two gaseous permeability values in the transverse direction are involved, one in the dry zone between the front position and the surface, and one in the wet zone, from the front to the center

$$A_1 = -\rho_v \frac{K_y^{\text{dry}}}{\mu_v} \qquad \text{and} \qquad A_2 = -\rho_v \frac{K_y^{\text{wet}}}{\mu_v} \tag{10}$$

The front temperature is connected to the vapor pressure through the liquid–vapor equilibrium and sorption isotherm relationships

$$P_{\text{front}} = P_1(x^* = L^*, y_1 = e) = P_{\text{vs}}(T_{\text{front}}) \times RH(X, T_{\text{front}}) \tag{11}$$

Here, both convective and radiative heat transfers are considered

$$\boldsymbol{q}_{c\,\text{ext}} = h\{T_{\text{ext}} - T_1(y_1 = 0)\} + \sigma\epsilon\{T_{\text{eq}}^4 - T_1^4(y_1 = 0)\} \tag{12}$$

where h is the heat-transfer coefficient, T_{ext} is the external temperature, σ is the Bolzmann constant, ϵ is the equivalent emissivity factor, and T_{eq} is the equivalent temperature for the radiative balance (which must account for the view factors to

Table 1. Parameter Values for the Three Different Kinds of Wood in the Simulations

	Properties	Softwood Sapwood	Softwood Heartwood	Beech
TransPore	Basic density ($kg \cdot m^{-3}$)	400	400	600
	Initial MC (%)	160	80	80
	Transverse gaseous permeability (m^2)	$4 \cdot 10^{-15}$	$2 \cdot 10^{-15}$	$1 \cdot 10^{-14}$
	Transverse liquid permeability (m^2)	$2 \cdot 10^{-14}$	$2 \cdot 10^{-15}$	$1 \cdot 10^{-14}$
	Longitudinal gaseous permeability (m^2)	$1 \cdot 10^{-12}$	$5 \cdot 10^{-13}$	$1 \cdot 10^{-10}$
	Longitudinal liquid permeability (m^2)	$5 \cdot 10^{-12}$	$5 \cdot 10^{-13}$	$1 \cdot 10^{-10}$
Front_2D	Permeability (m^2)	$4 \cdot 10^{-15}$	$2 \cdot 10^{-15}$	$1 \cdot 10^{-14}$
	Liquid diffusivity ($m^2 \cdot s^{-6}$)	$2 \cdot 10^{-6}$	$2 \cdot 10^{-7}$	$1 \cdot 10^{-6}$
	Wet/dry permeability ratio	0.5	0.1	0.5
	Anisotropy ratio	250	250	10 000

each of the external surfaces and their associated temperature value).

The moisture content profile and the liquid flux at the front position are given by

$$X_\ell = A\xi^2 + B\xi + C, \qquad \text{with} \qquad \xi = y_1 - e$$

$$\boldsymbol{q}_\ell = -a_{m\ell}\boldsymbol{\nabla}(X) = -\rho_\ell \frac{K_{y2}}{\mu_\ell}\frac{\partial P_c}{\partial X}\boldsymbol{\nabla}(X) = \langle q_m \rangle \boldsymbol{j} \qquad (13)$$

Assumption A9 implies that $B = \langle q_m \rangle / a_{m\ell}$. Obviously, according to the average moisture content, the initial moisture content, the irreducible saturation, and the mass flux, several cases have to be considered, and the full details of how to determine the constants A and C are also discussed in detail in Perré et al. (1999a).

In order to simulate the drying process using this semianalytical model, a computer code has been developed according to the set of equations proposed in the previous paragraphs. Due to the nonlinear expression of the external heat transfer and the effect of the drying rate on the front position, an efficient nonlinear solver has been used. It consists of a Newton-Raphson procedure, which procures a second-order convergence in the vicinity of the root. $Front - 2D$ is written in Fortran 90 and allows a complete drying simulation within a few seconds. Typically 2 s on a Pentium 800-MHz PC. Note that 50 terms are calculated in Eq. 9, although only a few (1 to 5) are usually required. This calculation time has to be compared with the time required when using the fastest two-dimensional version of *TransPore* (2-node flux approximation, structured mesh with Newton-Raphson procedure): between 2 and 5 min. The interested reader can obtain a detailed algorithm for the *Front_2D* model in Perré et al. (1999).

Parameter Values

Referring to the existing experimental data presented in Part I, three typical boards have been used in the present simulation work for comparison with experimental data: fir, sapwood; fir, heartwood; beech, sapwood.

The distinction between these boards arises from the set of physical parameters (Table 1) associated with each species. Most of the parameters given in Table 1 (density, initial moisture content, anisotropy ratios, gaseous over liquid permeability) are typical values measured for these kinds of wood samples (Agoua, 2001). For example, in the case of beech and the heartwood part of fir, the gaseous and liquid permeabilities have the same value. However, they are different for the sapwood part. Indeed, in the case of fir, pit aspiration occurs during drying for the sapwood part, but already has occurred before drying for the heartwood part (Comstock and Côté, 1968). Only one free parameter, the transverse gaseous permeability, has been adjusted in order to obtain a realistic duration for the first drying period that is comparable to the one observed during the experiment. This calibration procedure leads us to use values slightly higher than those usually measured. We already explained a plausible cause for this disagreement by the surface checking that usually occurs during the first falling drying-rate period, when only the peripheral zone of the section has entered the hygroscopic range. In the case of *Front_2D,* the same values of permeability have been used. However, in this case, the free parameter adjusted to obtain the right duration of the first drying period is the coefficient of liquid migration. The corresponding value (see Table 1) can be compared to the function of the Moisture Content obtained in the case of *TransPore,* when one assumes that the liquid migration due to the gradient of total pressure is negligible:

$$q_m = -\bar{\bar{a}}_{m\ell}\mathbf{grad}(X) = -\rho_0 \times \frac{\overline{\overline{K}}_\ell \cdot \bar{\bar{k}}_{r\ell}}{\mu_\ell} \times \frac{\partial P_c}{\partial X} \times \mathbf{grad}(X)$$

hence

$$\bar{\bar{a}}_{m\ell} = \rho_0 \times \frac{\overline{\overline{K}}_\ell \cdot \bar{\bar{k}}_{r\ell}}{\mu_\ell} \times \frac{\partial P_c}{\partial X} \qquad (14)$$

From the calculated function (Figure 4), it becomes obvious that the constant value to be used in *Front_2D* is close to the value of the function obtained for a low free water content (between 5% and 10%). This observation emphasizes the role of the very low value of the liquid migration coefficient obtained when the free water content decreases, which is a direct result of the shape of the relative permeability curve.

Finally, most of the key parameters that exist within the macroscopic transport equations (Eqs. 1–8) are strongly dependent on the structure of the material. These properties, together with their postulated functional dependencies, have been taken directly from the literature (see, for example, the comprehensive list of correlations supplied in Perré and Turner (1996) for the capillary pressure, relative permeability in the radial, transverse and longitudinal directions, vapor diffusivity,

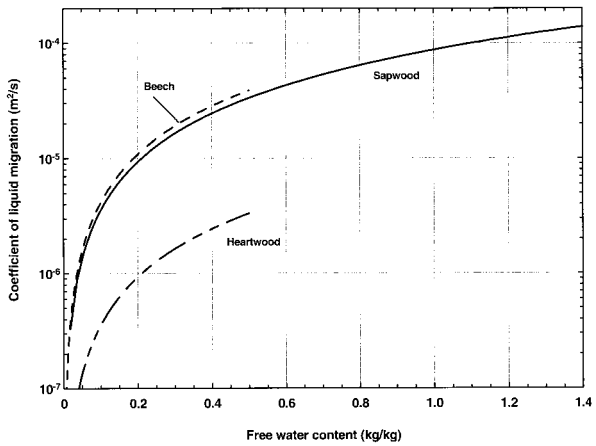

Figure 4. The liquid migration coefficient determined using the absolute permeability, the relative permeability curve, and the capillary pressure: The corresponding curves have to be compared to the constant values used in the semi-analytical model *Front_2D.*

and thermal conductivity) and are summarized in the Appendix.

Simulation Results

It is evident from Figures 5–7 that the simulation results computed using the full version of *TransPore* depict results whose trends are very similar to the experimental data reported in Part I. In particular, the results for fir sapwood shown in Figure 5 are especially close to test No. 15, with:

- A drying duration of approximately 500 min;
- An initial decrease of internal overpressure;
- A distinct duration of the first drying period ($T = T$ boiling 60°C and an overpressure almost equal to zero);
- A rapid increase in temperature during the second drying stage with a corresponding overpressure (same order of magnitude: 0.3 bar).

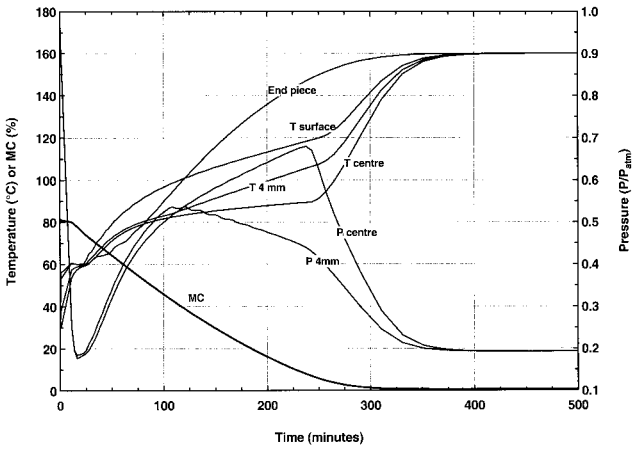

Figure 6. Simulation results obtained with the comprehensive model *Transpore:* heartwood part of fir; averaged MC, temperature, and total pressure at different positions plotted vs. time.

Compared to the previous test for sapwood, one has to note for fir heartwood in Figure 6 (both in the simulation results and the experimental data, tests 6 and 13) the following important observations:

- There is no constant drying stage;
- The initial pressure decrease meets the pressure increase during the second drying stage;
- No temperature plateau is evident at the boiling point of water;
- A higher overpressure is generated for heartwood (about 0.5 bar);
- The duration of drying is comparable (400 min) to that needed for sapwood, which has a much higher initial moisture content.

The results presented for beech in Figure 7 exhibit the same behavior as fir sapwood, except that a very low pressure level is evident. Again, this is consistent with the experimental data reported in Part I (tests Nos. 7 and 10). Note, in this case, the

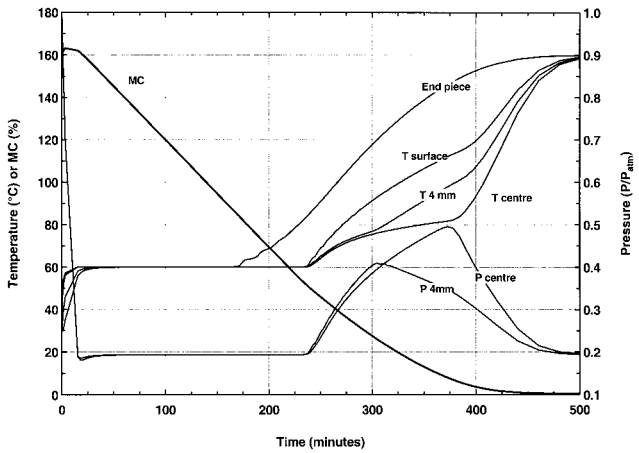

Figure 5. Simulation results obtained with the comprehensive model *Transpore:* sapwood part of fir; averaged MC, temperature, and total pressure at different positions plotted vs. time.

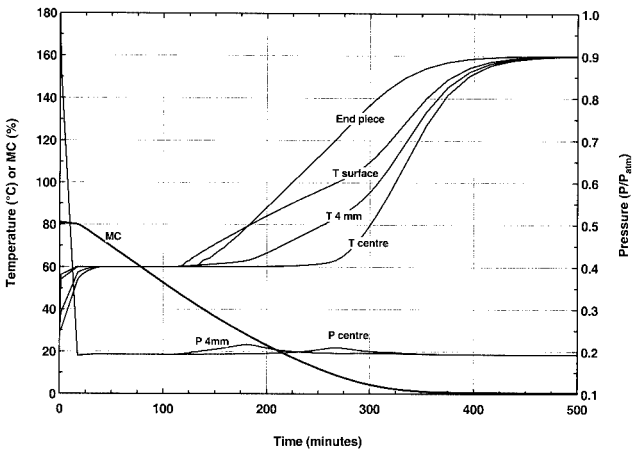

Figure 7. Simulation results obtained with the comprehensive model *Transpore:* beech, averaged MC, temperature, and total pressure at different positions plotted vs. time.

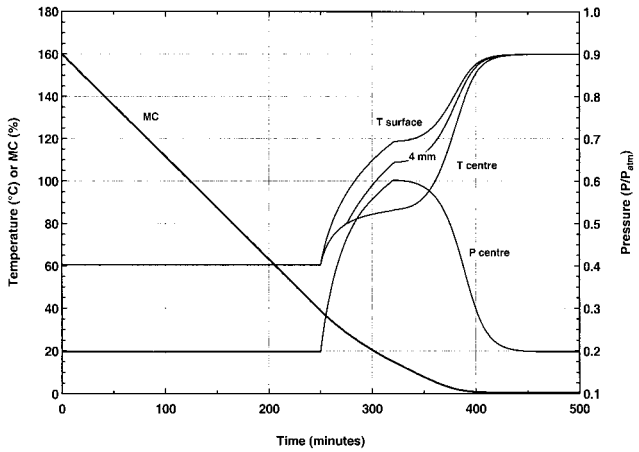

Figure 8. Simulation results obtained with the semianalytical model *Front_2D:* sapwood part of fir; averaged MC, temperature at different positions, and center pressure plotted vs. time.

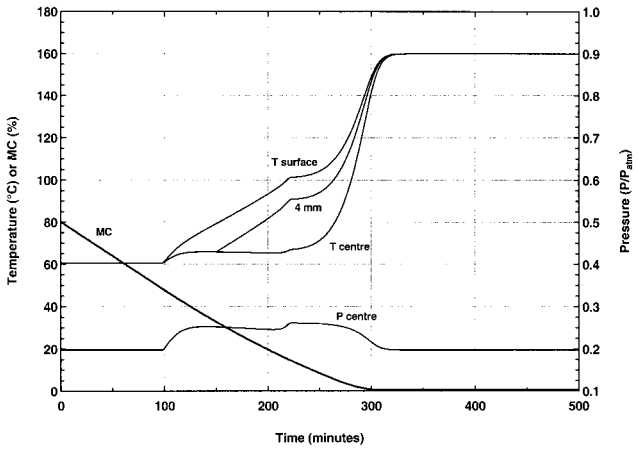

Figure 10. Simulation results obtained with the semianalytical model *Front_2D:* beech, averaged MC, temperature at different positions, and center pressure plotted vs. time.

difference of duration between the constant drying-rate period (125 min) and the period during which the center temperature remains very close to the boiling point of water (275 min.). This phenomenon is due to the very high permeability value of beech. A coarse analysis of the experimental data could have led to the conclusion that the constant drying-rate period in this case was approximately 275 min.

The simulation results for *Front_2D* are depicted in Figures 8–10. Clearly, as expected due to the numerous simplifying assumptions used to derive the model, these results are not as accurate as those observed for *TransPore.* Nevertheless, the trends in the results are all similar to those reported in the experiments. Note, however, that *Front_2D* is unable to simulate the initial pressure decrease.

The results for the drying of sapwood are shown in Figure 8. Specifically, one sees it remain a long time at the constant drying rate period, a rapid temperature increase, which is, in fact, too rapid compared with the experimental data, and a relatively high overpressure level of 0.4 bar. These results should be compared with those given in Figure 5, where it can be seen that the temperature increase spans a period of around 300 min, as opposed to 150 and a smaller, more realistic overpressure of 0.3 bar for the experiment, or for *TransPore.* Finally, note that the overall drying times are roughly the same for the two models.

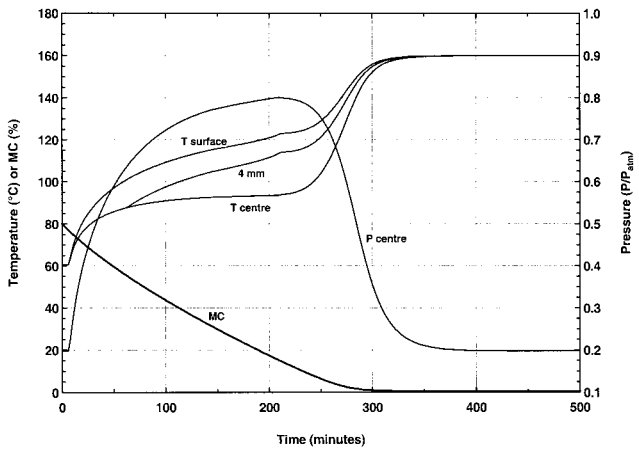

Figure 9. Simulation results obtained with the semianalytical model *Front_2D:* heartwood part of fir; averaged MC, temperature at different positions, and center pressure plotted vs. time.

The simulation results for the drying of heartwood computed using the semianalytical model are given in Figure 9. These results should be compared with Figure 6, which is computed using the comprehensive model. Here a very short first drying period is evident, and one can see that the overpressure level initially increases too quickly and attains a value that is higher than is evident in either *TransPore* or the experiment—0.6 bar against 0.5 bar for the experiment. The temperature increase is again quite rapid in comparison with the experiment.

In Figure 10 one again can observe that using the semianalytical model results in quite good trends in comparison with the simulation results reported for *TransPore* in Figure 7 and the experiments. In particular, the same mechanisms are shown, namely, a constant drying-rate period of 100 min. and a period of approximately 300 min. at the boiling point, a low overpressure level- and a too-rapid increase in temperature, especially between 250 and 300 min. This fact can be a consequence of the chosen moisture-content gradient during drying, especially because we assume the liquid-migration coefficient to be constant whatever the free moisture content.

Figures 11 and 12 depict the moisture-content fields computed using *TransPore* for the three boards under investigation after 1 and 2 h of drying, respectively. The strong longitudinal moisture transfer allows only the assumption of MC gradient in the transverse direction to be verified (assumption A8). Except for the very end piece of heartwood, the moisture content does not depend on the longitudinal position.

Conclusions and Prospects

In Part II of this research work, two mathematical models have been used to simulate the vacuum drying of wood with radiative heating. One model (*TransPore*) is more comprehen-

sive than the other (*Front_2D*) and is able to capture quite subtle transport mechanisms, including the initial decrease of pressure, which requires an accurate air balance within the wood. However, both models capture the overall trends of the global drying behavior evident in the experimental data reported in Part I. In particular, both are able to identify the large differences in drying behavior between boards cut from different species of wood.

In conclusion, it is clear from this work that the simpler model (*Front_2D*) is able to provide a reasonable account of the wood vacuum drying process, and most importantly, allows the simulations to be performed within a few seconds. Clearly, such a model would be suitable for on-line kiln control of vacuum processes where the drying behavior of a stack of timber, which contains a variety of sapwood and heartwood

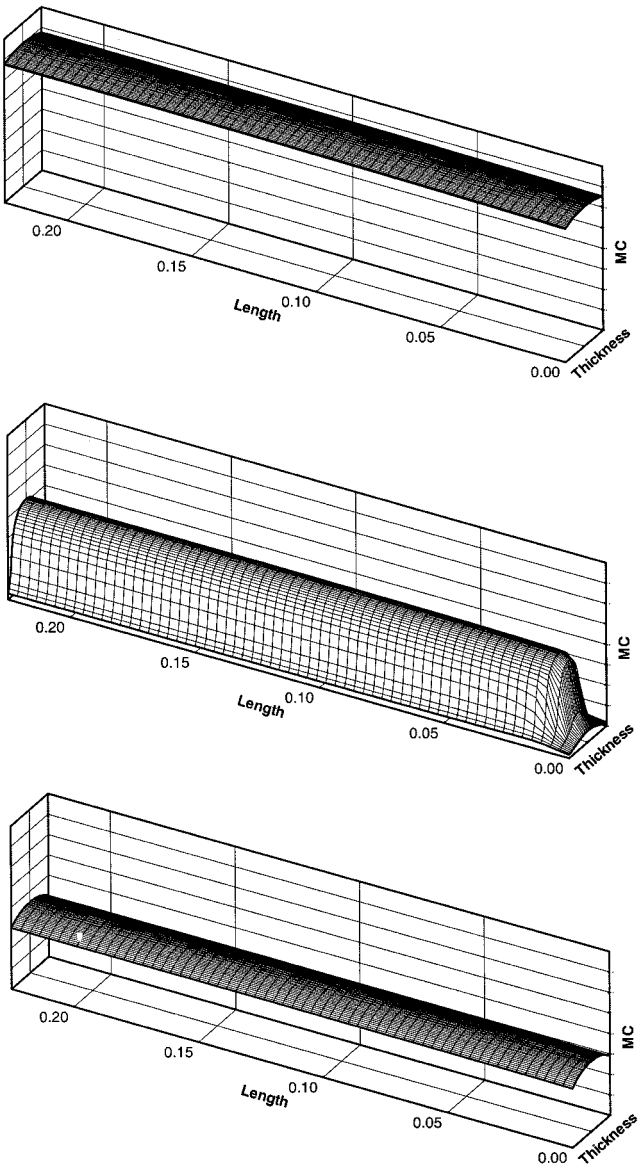

Figure 11. Comprehensive model *Transpore: 2-D* moisture content fields calculated at 1 h of drying for fir (sapwood and heartwood) and for beech.

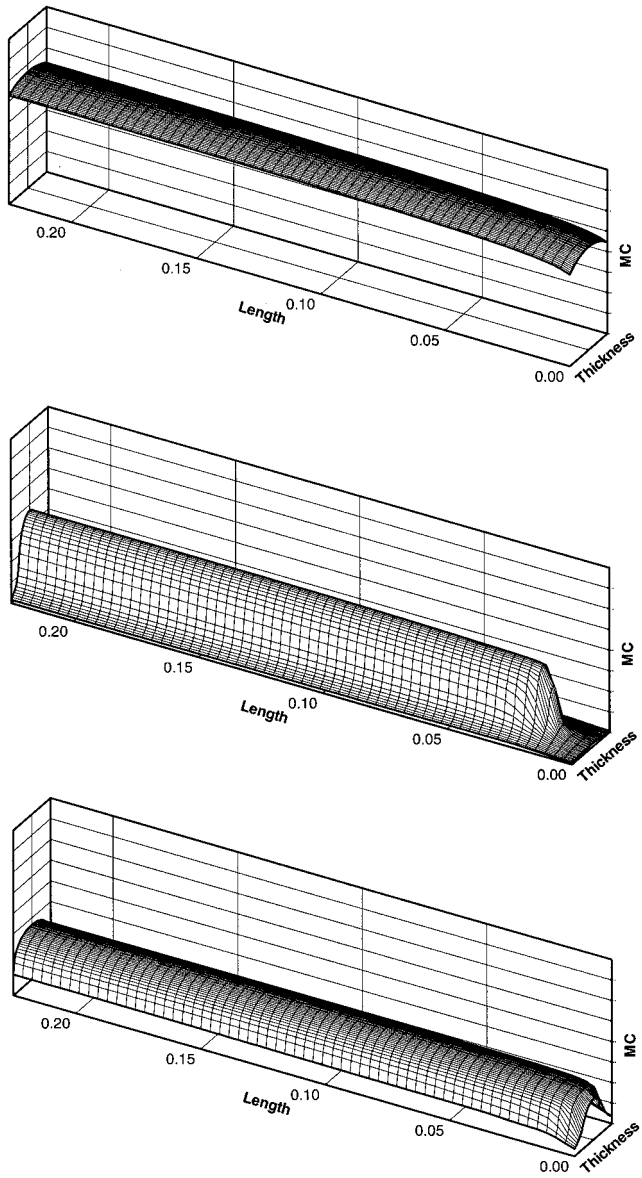

Figure 12. Comprehensive model *Transpore: 2-D* moisture content fields calculated at 2 h of drying for fir (sapwood and heartwood) and for beech.

boards, would be required simultaneously. Such a complex configuration would be a substantial computational challenge for the comprehensive model. Furthermore, in opposition to the comprehensive formulation, *Front_2D* also allows the drying behavior to be simulated using very few constant parameters. This is very informative in terms of the important physical mechanisms involved in vacuum drying. In addition, this led to a dramatic simplification of the product characterization (a difficult and tedious task) when the accuracy level produced by *Front_2D* is sufficient. On the other hand, if accuracy is foremost, then the comprehensive model (*TransPore*) cannot be surpassed. Given that computational power is always on the increase, and large strides are always being made in computational science, one can only imagine that the computational

requirements of the comprehensive model will only decrease in the future.

Acknowledgments

The authors to acknowledge the funding from an Australian Research Council Large grant scheme in association with Prof. Victor Rudolph, Department of Chemical Engineering at University of Queensland, that supported some of this research work.

Literature Cited

Agoua, E., "Diffusivité et Perméabilité du Bois: Validation de Méthodologies Expérimentales et Prise en Compte de Paramètres Morphologiques Simples pour la Modélisation Physique," PhD Diss., ENGREF, Nancy, France (2001).

Ben Nasrallah, S., and P. Perré, "Detailed Study of a Model of Heat and Mass Transfer During Convective Drying of Porous Media," *Int. J. Heat Mass Transfer,* **31,** 957 (1988).

Boukadida, N., and S. BenNasrallah, "Two-Dimensional Heat and Mass Transfer During Convective Drying of Porous Media," *Drying Technol.,* **13**(3), 661 (1995).

Bird, R. B., W. E. Stewart, and E. N. Lightfoot, *Transport Phenomena,* Wiley, New York (1960).

Bramhall, G., "Mathematical Model for Lumber Drying," *Wood Sci.,* **12**(1), 14 (1979).

Comstock, G. L., and W. E. Côté, "Factors Affecting Permeability and Pit Aspiration in Coniferous Sapwood," *Wood Sci. Techn.,* **2,** 279 (1968).

Crank, J., *The Mathematics of Diffusion,* Oxford Univ. Press, Oxford (1975).

Doe, P. E., A. R. Oliver, and J. D. Booker, "A Non-Lineal Strain and Moisture Content Model of Variable Hardwood Drying Schedules," 4th Proc. IUFRO Wood Drying Conf., Rotorua, New Zealand, 203 (1996).

Fyhr, C., and A. Rasmuson, "Numerical Simulation of Superheated Steam Drying of Wood Chips," *AIChE J.,* **42,** 2491 (1996).

Hadley, G. H., "Theoretical Treatment of Evaporation Front Drying," *Int. J. Heat Mass Transfer,* **25**(10), 1511 (1982).

Ilic, M., and I. W. Turner, "Convective Drying of a Consolidated Slab of Wet Porous Material," *Int. J. Heat Mass Transfer,* **32,** 2351 (1989).

Kawai, S., *Moisture Movement and Drying Stresses in Wood,* PhD Diss., Faculty of Agriculture, Kyoto University, Japan (1980).

Keey, R. B., T. A. L. Langrish, and J. C. F. Walker, *The Kiln-Drying of Lumber,* Springer-Verlag, Berlin (2000).

Moyne, Ch., *Transferts Couplés Chaleur-Masse lors du Séchage: Prise en Compte du Mouvement de la Phase Gazeuse,* Thèse de Doctorat d'Etat, INPL, Nancy, France (1987).

Pang, S., "Moisture Content Gradient in a Softwood Board During Drying: Simulation from a 2-D Model and Measurement," *Wood Sci. Technol.,* **30,** 165 (1996).

Perré, P., and A. Degiovanni, "Simulation par Volumes Finis des Transferts Couplés en Milieux Poreux Anisotropes: Séchage du Bois à basse et à Haute Température," *Int. J. Heat Mass Transfer,* **33**(11), 2463 (1990).

Perré, P., M. Moser, and M. Martin, "Advances in Transport Phenomena During Convective Drying with Superheated Steam or Moist Air," *Int. J. Heat Mass Transfer,* **36**(11), 2725 (1993).

Perré, P., and I. W. Turner, "Using a Set of Macroscopic Equations to Simulate Heat and Mass Transfer in Porous Media: Some Possibilities Illustrated by a Wide Range of Configurations that Emphasize the Role of Internal Pressure," *Numerical Methods and Mathematical Modelling of the Drying Process,* I. W. Turner and A. Mujumdar, Dekker, New York, p. 83 (1996).

Perré, P., and I. W. Turner, "Microwave Drying of Softwood in an Oversized Waveguide," *AIChE J.,* **43**(10), 2579 (1997).

Perré, P., I. W. Turner, and J. Passard, "2-D Solution for Drying with Internal Vaporization of Anisotropic Media," *AIChE J.,* **45**(1), 13 (1999).

Perré, P., and I. Turner, "*TransPore:* A Generic Heat and Mass Transfer Computational Model for Understanding and Visualising the Drying of Porous Media," *Drying Technol.,* **17**(7), 1273 (1999a).

Perré, P., and I. Turner, "A 3D Version of *TransPore:* A Comprehensive Heat and Mass Transfer Computational Model for Simulating the Drying of Porous Media," *Int. J. Heat Mass Transfer,* **42**(24), 4501 (1999b).

Rogers, J. A., and M. Kaviany, "Funicular and Evaporating-Front Regimes in Convective Drying of Granular Beds," *Int. J. Heat Mass Transfer,* **35**(2), 469 (1992).

Siau, J. F., "Transport Processes in Wood," Springer-Verlag, Berlin (1984).

Stanish, M. A., G. S. Schajer, F. Kayihan, "A Mathematical Model of Drying for Hygroscopic Porous Media," *AIChE J.,* **32**(8), 1301 (1986).

Turner, I., and P. Perré, "A Synopsis of the Strategies and Efficient Resolution Techniques Used for Modelling and Numerically Simulating the Drying Process," *Numerical Methods and Mathematical Modelling of the Drying Process,* I. W. Turner and A. Mujumdar, eds., Dekker, New York, p. 1 (1996).

Turner, I. W., and P. Perré, "The Use of Implicit Flux Limiting Schemes in the Simulation of the Drying Process: A New Maximum Flow Sensor Applied to Phase Mobilities," *Applied Mathematical Modelling,* Vol. 25, Elsevier, Amsterdam, The Netherlands, 513 (2001).

Van Meel, D. A., "Adiabatic Convection Batch Drying with Recirculation of Air," *Chem. Eng. Sci.,* **9,** 36 (1958).

Whitaker, S., "Coupled Transport in Multiphase Systems: A Theory of Drying," *Advances in Heat Transfer,* **31,** 1 (1998).

Appendix: Values Used in the Computations

All values that depend on the board under consideration are listed in Table 1 of the text. Values for the tests are given in Table A1.

Table A1. Test Configuration

Parameter	Value
Equivalent temperature	$T_{eq} = 160°C$
Equivalent emissivity	$\epsilon = 0.8$
Heat-transfer coefficient	$h = 0$*
Half-length	250 mm
Half-thickness	13 mm

* Convective heat transfer is neglected in all simulations presented in this article.

Physical parameters used in TransPore

Because wood is highly hygroscopic, bound water has to be separated from free water:

$$X = X_b + X_{fw},$$

where

Table A2. Scalar Values

Material Properties	Values Used for the Computations
Heat capacity	$\overline{\rho C_p} = \rho_0(1113 + 4.85T + 4185X)\ (\mathrm{J \cdot kg^{-1} \cdot K^{-1}})$
Sorption isotherm	$\frac{P_V}{P_{VS}} = 1 - \exp(-0.76427A - 3.6787A^2)$ with $A = X_b/X_{fsp}$
Capillary pressure	$P_c = 1.24 \times 10^5 \sigma(S_{fw} + 1 \times 10^{-4})^{-0.61}$

Table A3. Tensorial Values

Material Property	Transverse	Longitudinal
Gaseous diffusion	$D_{\text{eff}}^{T} = 4.10^{-3} \times k_{rg} \times D_V$	$D_{\text{eff}}^{L} = 4.10^{-2} \times k_{r\ell} \times D_V$
Bound water diffusion	$D_b^T = \left[-9.9 + 9.8X - \frac{4300}{T_k}\right]$	$D_b^L = 2.5 \times D_b^T$
Thermal conductivity	$\lambda_{\text{eff}}^{T} = 0.14 + 0.3 \times X$	$\lambda_{\text{eff}}^{L} = 2 \times \lambda_{\text{eff}}^{T}$
Liquid relative permeability	$k_{r\ell}^{T} = (S_{wf})^3$	$k_{r\ell}^{L} = (S_{wf})^8$
Gaseous relative permeability	$k_{rg}^{T} = 1 + (2S_{wf} - 3)(S_{wf})^2$	$k_{rg}^{L} = 1 + (4S_{wf} - 5)(S_{wf})^4$

Table A4. Physical Parameters Used in Front_2D

Material Property	Value
Thermal conductivity (λ)	0.15 W · m · °C^{-1}
Fiber saturation point	30%
Irreducible MC (X_{irr})	30%

$X_b = min(X_{fsp}, X)$ and $X_{fsp} = 0.325 - 0.001T$

(at full saturation, $X_{sat} = X_{fsp} + X_{fw\ max}$).

The saturation variable involved in the relative permeability functions is calculated according to the free water content only:

$$S_{fw} = \frac{X_{fw}}{X_{fw\ max}}.$$

The values are given in Tables A2 and A3.

Although the FSP value does decrease with temperature, from about 30% at room temperature down to about 20% at 100°C (Siau, 1984), a constant value has been used in *Front_2D* (see Table A4). This could be included in the code, but would lead to little changes.

Manuscript received June 19, 2002, revision received May 24, 2003, and final revision received Aug. 11, 2003.